An Effective Ultrasound Acoustic Measurement to Monitor the Lithium-ion Battery Electrode Drying Process with Various Coating Thicknesses

Ye Shui Zhang[*1,2,3], James B. Robinson[1,2], Rhodri E. Owen[1,2], Anand N. P. Radhakrishnan[1], Juntao Li[1,2], Jude O. Majasan[1], Paul R. Shearing[1,2], Emma Kendrick[2,4], Dan J.L. Brett[*1,2]

[1.] Electrochemical Innovation Lab, Department of Chemical Engineering, University College London, London, UK WC1E 7JE

[2.] The Faraday Institution, Quad One, Harwell Science and Innovation Campus, Didcot, UK OX11 0RA

[3.] School of Engineering, University of Aberdeen, Aberdeen, AB24 3UE, UK

[4.] School of Metallurgy and Materials, University of Birmingham, Birmingham, UK B15 2TT

(Corresponding author: d.brett@ucl.ac.uk; yeshui.zhang@ucl.ac.uk)

Keywords: LIBs, electrode drying process, ultrasound acoustic measurement, drying mechanism, drying dynamics

Abstract

The electrode drying process is a crucial step in lithium-ion battery manufacturing chain, and plays a fundamental role in governing the performance of the cells. The drying process is extremely complex, with the dynamics and their implication in the production of electrodes generally poorly understood. To date there is limited discussion of these processes in the literature due to the limitation of existing *in-situ* metrology. Here, ultrasound acoustic measurements are demonstrated as a promising tool to monitor the physical evolution of the electrode coating *in-situ*. These observations are validated by gravimetric analysis to show the feasibility of the technique to monitor the drying process and identify the three different drying stages. A possible application of using this technique is to adjust the drying rates based upon the ultrasound readings at different drying stages, to speed up the drying time. These findings prove this measurement can be used as a cost-effective and simple tool to provide characteristic diagnostics of the electrode, which can be applied in large scale coating manufacturing.

1 Introduction

Lithium-ion batteries (LIBs) have been widely applied in portable electronic devices and state-of-the-art electric vehicles due to their high energy and power densities. The high demand of LIBs has led to an exponential increase in battery manufacturing with a current market size of $34.2 billion[1]. The size is expected to grow at a compound annual growth rate of 13.0% from 2020 to 2027[1]. To maintain consistency of the electrodes within a cell, a standardised and

defect-free electrode layer is required; this allows uniform current density and lithium-ion transport between electrodes, reducing battery degradation and failure. Optimising the porous structure and physical, mechanical and electrochemical properties of these electrode films are imperative in maintaining good consistency and electrochemical performances in the final cell. These factors are controlled through the mixing, coating, drying and subsequent calendering process. Despite a recent rise in interest in the electrode drying process (DP) in the literature[2-13], the drying dynamics of wet electrode films are complex and poorly understood. To better control and optimise the electrode structure and properties throughout the DP, it is necessary to develop new drying methodologies and analysis techniques to understand solvent evaporation effects on crack formation and the promotion of self-assembly processes[14]. Zhang *et al.*[14] have comprehensively reviewed the drying effects on the LIB electrodes with the critical discussion about the drying mechanism and models. This highlights the necessity and the challenges for developing novel metrology, which could be used as tools to monitor and predict the electrode quality *in-situ*. In addition, greater control of the electrode DP and cutting-edge diagnostic techniques are required to enable *in-situ* characterization of the electrode during drying[15-18].

Typically, investigations have focussed on *ex-situ* characterisations as a result of the limitations of current characterisation techniques. These *ex-situ* studies include analysing the morphology of the electrode coating, microstructure of the dried electrodes, elemental distribution through the coating, microstructure of the particles, pore size distribution across the electrode coating and thickness of electrode films[2, 8-9, 19-28]. However, *in-situ* characterisation methods, which have been rarely used to study the DP, offer the opportunity for greater *in-line* control. There are limited number of techniques have been used in the electrode DP to investigate the microstructural evolution, for example thecontrast-variation small-angle neutron scattering can perform a structural evaluation of a catalyst ink for polymer electrode fuel cell electrodes[27], drying rate with thermogravimetric analysis (TGA)[2], binder distribution[2-3, 6, 12, 27, 29]with Raman spectroscopy[4], particle distributions with X-ray Radiography[30], carbon black identification with an energy-selective back detector[12], and stress development with a Cantilever deflection method [29]. However none of these techniques can be easily incorporated into a coating line, for effective *in-line* control. There is an urgent need to develop an effective and simple *in-situ* tool which can specifically be used in the LIB manufacturing chain.

Ultrasound acoustic-based techniques have shown the advantages to monitor batteries during operation[31]. For example, Hsieh *et al.*[32] validated the viability of using ultrasound acoustic technique to understand the physical dynamics of cells under change and discharge conditions by interpreting the time-of-flight (ToF) of acoustic signals. Davies *et al.*[33] reported

the evolution of the ultrasonic signals at transmission mode is caused by the revolution of coating layer density and bulk modulus. Robinson *et al.*[34] spatially mapped the change in condition of electrodes for a cell phone battery with ultrasound acoustic measurement during cycling. Deng *et al.*[35] improved an ultrasound imaging method to understand the internal revolution of a pouch cell non-destructively by recording its acoustic signal transmittance. This work revealed the potential to observe the electrolyte wetting of cells more accurately to identify the battery failure mechanism. In a recent review, Majasan *et al.*[31] highlighted some of the key challenges and potential for extending the commercial applications of acoustic diagnostics.

Recently, the drying dynamic evolution with a ultrasound acoustic measurement was investigated[36], the acoustic signal attenuation were used to designate the evolution of the electrode coating film's physical properties.The ultrasound signal evolution has been well studied to correlate with the reported three-stage drying mechanism, which also indicate the evolution of current collector to electrode coating interface.The density of the electrode coating increases during the DP, that result in a faster response of the ToF[36]. The investigations highlight the efficiency of acoustic-based techniques as an *operando* metrology to investigate the physical property evolution during the LIB DP.

To further optimize the industrial electrode manufacturing process, the cost of drying must be taken into account, with the DP being shown to be one of the most energy intensive steps needed to fabricate LIBs[37]. It has been reported that ~47% of the total process energy can be attributed to the electrode DP with a significant portion of this needed to enable solvent evaporation and recovery[38]. As noted by Li *et al*.[39], improving the electrode manufacturing process to reduce both cost and energy consumption is a significant challenge. Therefore, there is emerging need to develop an *in-situ* metrology to monitor the drying status in real time to produce cost-effective electrodes. This work incorporates gravimetric analysis alongside ultrasound acoustic measurements, validating the assumptions obtained from the ultrasonic signals and demonstrating the ability of the ultrasonic technique to obtain information not available from traditional gravimetric analysis alone. This work provides an outlook on the utility of ultrasound acoustic measurement tool to effectively monitor the electrode DP, offering the potential to employ the technique within LIB manufacturing to control and optimise the electrode manufacturing.

2 Materials and experimental set-up

The raw materials and the formulation of the anodes with different coating thicknesses (200, 250, 300 and 350 µm thick wet slurry coatings) prepared for this study are reported in previous

work[36]. The coatings were dried for varying lengths of time at room temperature (RT) to acquire ultrasound acoustic signals.

All ultrasound acoustic measurements for investigating the DP of anode slurry coating with different thicknesses (200, 250, 300 and 350 µm) were carried out using the same Olympus Epoch 650 ultrasonic flaw detector (Olympus Corp., Japan)as reported before [36].. The experimental setup and schematic diagram are shown in Figure 2 (a) and (d), respectively. To acquire the ultrasound acoustic signals during the DP, the transducer was placed underneath the current collector (with the electrode slurry coating on the upper side of the current collector) with a thin layer of Couplant D ultrasonic gel (Olympus Corp., Japan) between the transducer and the current collector. In Figure 2 (b) and (c), an aluminium holder was designed to mount the transducer to provide a good contact between transducer and the current collector, and also enable to have a stable gravimetric reading. Measurements were carried out using a range of acoustic gain between 40-70 dB with no delay imposed on the measurements. This settings of the Olympus Epoch 650 ultrasonic flaw detector is similar to work reported previously[36]. Schematic diagrams of ultrasonic reflection of electrode, reflected paths of ultrasonic waves through a wet slurry electrode coating with solvent, the reflected paths of ultrasonic waves through dried solid electrode (without solvent) and the interfaces in electrode DP are shown in Figure 1.

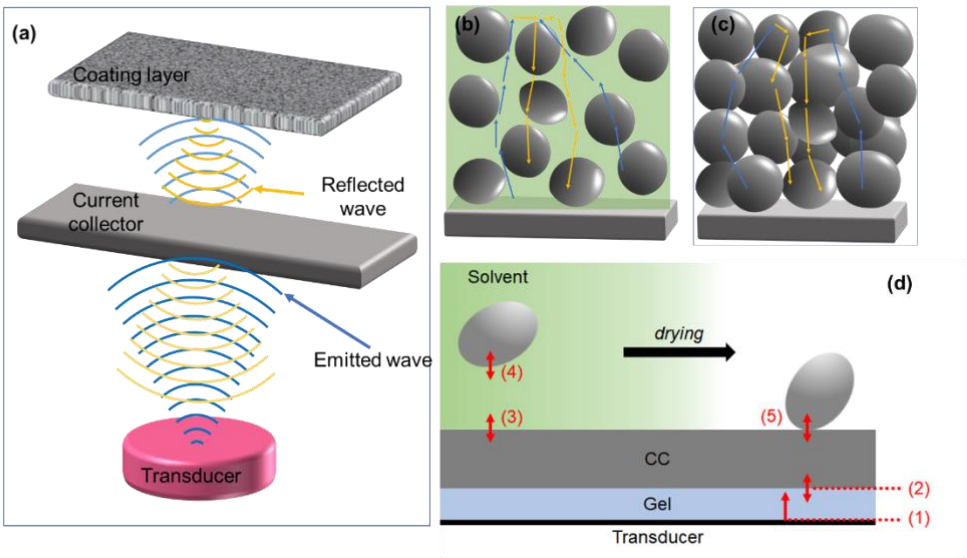

Figure 1 Schematic diagrams (a) Ultrasound acoustic signal reflections through the electrode layer; (b) Reflected paths of ultrasonic waves through a wet slurry electrode.; (c) reflected paths of ultrasonic waves through dried solid electrode.; (d) interfaces in electrode drying process, which ToF shifts occur as interfaces (3) - (4) diminishes and transits to interface (5) [Adapted with permission from [36]. Copyright {2021} American Chemical Society.]

To obtain the most reliable signal response for the initial interface layers without saturating the receiver (also the same transducer), the range of gain was determined manually to ensure the

acoustic response is close to 100%. The resolution of the output of the acoustic reading is ~2.5 ns. The Epoch 650 ultrasonic flaw detector was controlled in a same way as reported before[36].

To confirm the reliability of the ultrasound acoustic measurement as an effective tool to monitor the electrode DP, gravimetric analysis was conducted concurrently using the set-up shown in Figure 2 (a) and (d). A KERN PNJ 600-3N balance with a KERN Balance Connection software was used to record the weight change during DP. The acoustic signals were recorded over the entire DP with 0.5 min interval until stable signal were observed and also no weight change from the gravimetric reading. A thermocouple was attached to the surface of the transducer holder to monitor the temperature during the investigation using a TC-08 temperature data logger (Pico Technology, UK) and PicoLog 6 software (Pico Technology, UK). Each experiment with different slurry coating thickness was repeated to ensure reproducibility of the results.

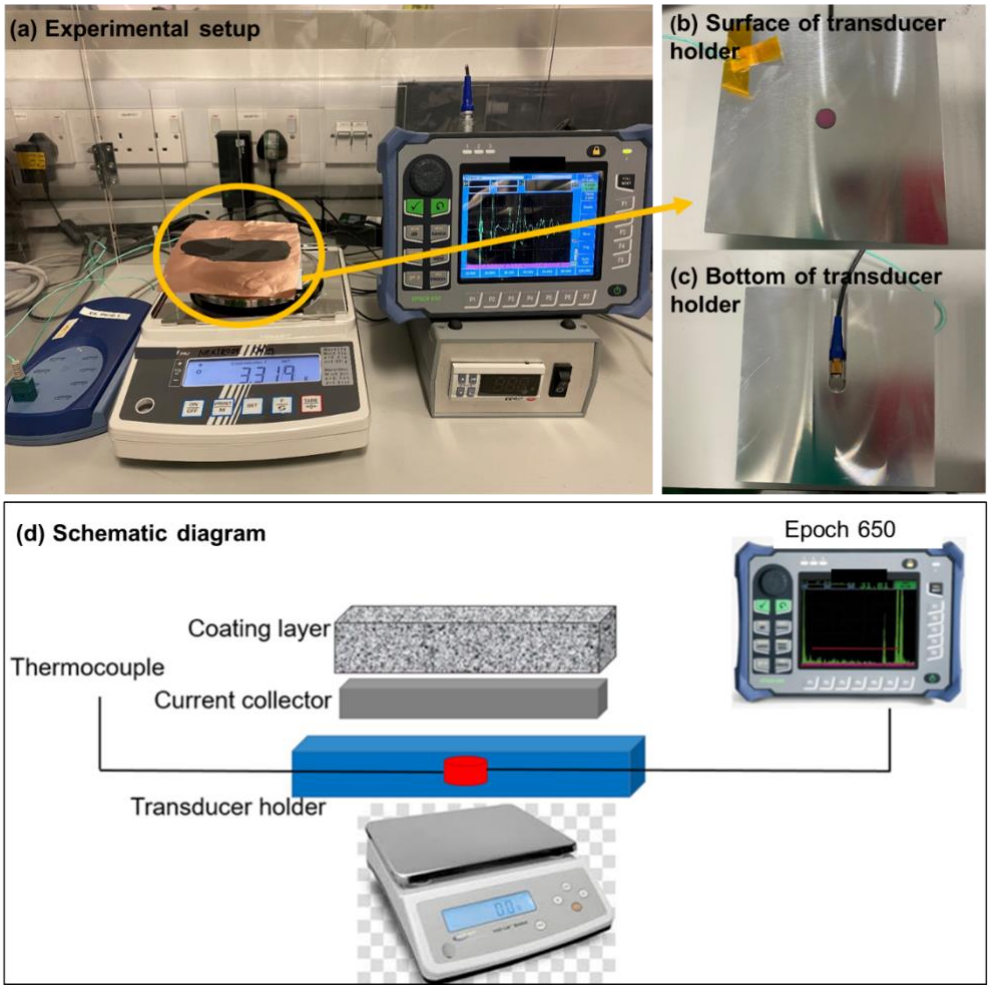

Figure 2 Experimental set-up for using ultrasound acoustic technique to study thermal dynamic during electrode drying process: (a) Image of the set-up; (b) Surface of the transducer holder; (c) Bottom of the transducer holder; (d) Schematic diagram of the set-up.

3 Results and discussion

3.1 Ultrasound acoustic signal interpretation

The principles of pulse-echo ultrasound acoustic measurements to analyse electrode DP have been discussed in detail previously[36]. The reflected waves at each interface or region of significant change in acoustic properties and the subsequent reflection wave recorded by the same transducer which was also emitting the ultrasound wave. The ultrasound wave is mechanical wave which needs conductive medium to propagate the transmission of the wave primarily occurs *via* the liquid in a wet electrode. This results in a dynamic response in the ultrasonic signal which can be correlated to the DP as the solvent is removed from the electrode slurry[36].

Figure 3(a), is an example acoustic signal received at the beginning of drying a 200 µm anode slurry coating. The 1st ToF signal between 1.0-2.5 µs is indicating multiple reflective paths taken by the ultrasound waves, which are reflecting the different interfaces of the electrode. With the grouping identified as the 2nd round of signals, between 2.5-4.0 µs, being echoes of the same reflection peaks; therefore, the data processing will only focus on the 1st round of signal with multiple peaks as shown in Figure 3(b). To further quantify the dynamic information from the acoustic signals acquired during DP, the Δ ToF and Δ Intensity are calculated as shown in Figure 3 (c), which indicate changes in the interface from 0 to 90s during the electrode DP is consistent with a contraction in the electrode film.

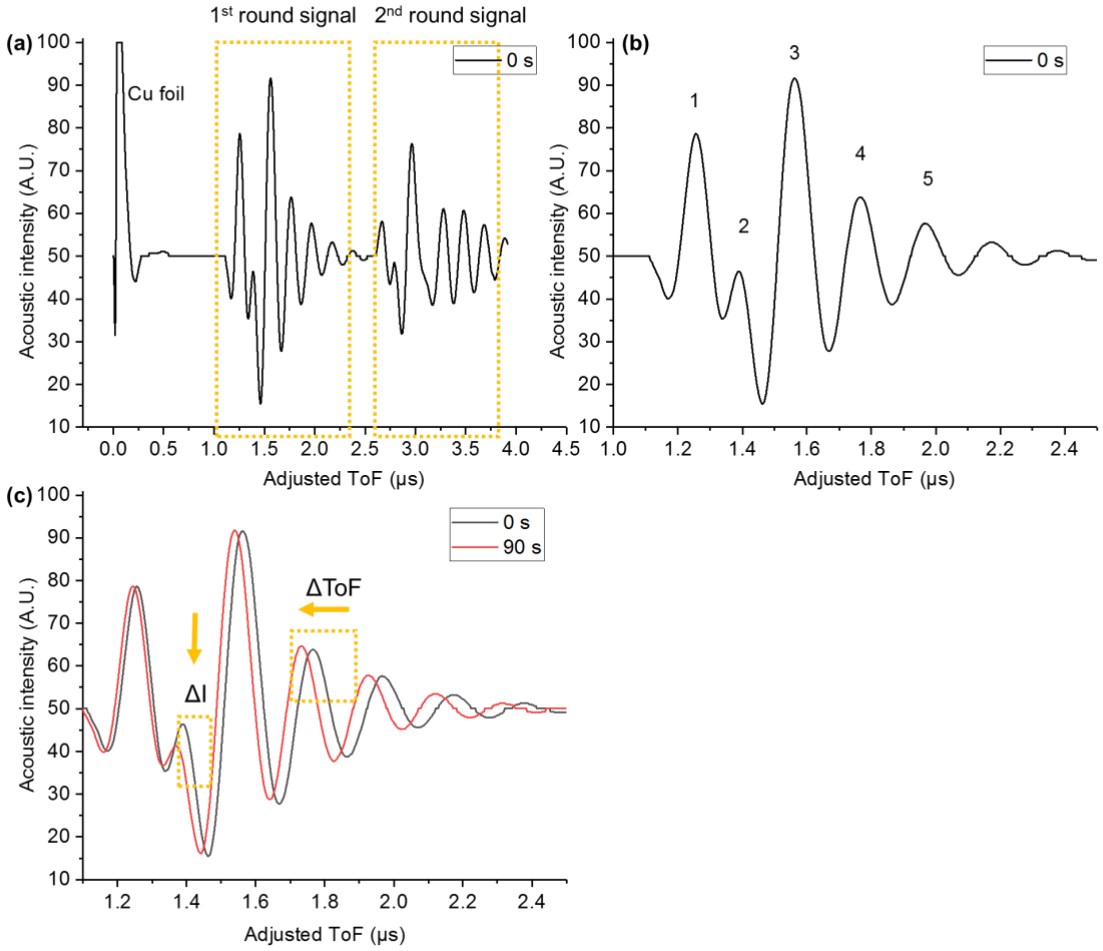

Figure 3 (a) Acoustic signals received at the initial stage of drying 200 μm anode slurry at RT with two rounds of signal; (b)1st round of signal with peak numbering; (c) Defined delta intensity and ToF of the acoustic signal. The adjusted ToF are aligned after similarity analysis, and the details are described in published work[36].

3.2 Time-of-flight evolution during the electrode drying process

The ultrasound acoustic signal response acquired during electrode DP can be analysed in two ways, the first, a colour map which demonstrates the evolution of ToF as a function of the drying time is shown in Figure 4(a), Figure 5(a), Figure 6(a) and Figure 7(a), and a second which (shown in Figure S1) illustrates the acoustic signal evolution for each peak.

Figure 4(a), Figure 5(a), Figure 6(a) and Figure 7(a) show the 2D ToF maps of anode drying with coating thickness at 200, 250, 300 and 350 μm. The results show a similar signal evolution during the DP regardless the coating thickness, with a clear change in the signal intensities which can be related to the changes in film density and composition at different stages of the DP. The 1st stage of the DP shows a strong decrease in the ToF observed for the acoustic signals due to the solvent evaporating and the film shrinking. The ToF evolution in the 2nd stage is less significant than that seen in the 1st stage, although again the ToF can be seen to continue to contract before the relative stability of the 3rd stage is seen. It is noticeable there

is a fluctuation period between 2nd and 3rd stage for all coatings. The detailed interpretation will be discussed in the next sections.

Stage 1: The solvent evaporates , as the solvent continuing evaporates from the surface of the electrode coating, an increasing volume of solvent is transported towards the surface *via* capillary action. The majority of the pore emptying, which is observed during the DP, is governed by solvent evaporation which creates a gradient in the surface tension known as Marangoni flow. The liquid flow is expressed by Darcy's law (permeability multiplied by the gradient of capillary pressure)[40] as shown in Equation 1, that can be described as the absence of gravitational forces and in a homogeneously permeable medium, is given by a simple proportionality relationship between the instantaneous flux, where k is the permeability of the medium, the μ is the dynamic viscosity of the fluid, and Δp is the pressure drop over a given distance L[41-42]. Figure 3 shows that in the 1st stage, for each thickness of coating, the peak signal occurs at reducing ToF, and the rate at which this decreases is related to the thickness of the coating, and the consolidation of the film as the solvent is removed.

$$q = -\frac{k}{\mu L}\Delta p \qquad \text{Equation 1}$$

Stage 2: The removal of solvent from the regions between the active material particles result in a constriction in the volume of the electrode as the particles move closer.. The pressure gradient throughout the electrode coating causes efficient suction from the pores due to capillary pressure, as described by Young-Laplace equation[9]. As shown in Equation 2, Young-Laplace equation relates the pressure difference to the shape of the surface or wall and it is fundamentally important in the study of static capillary surfaces, where p_c is capillary pressure, σ is surface tension and the principal radii of curvature, R_1 and R_2[43]. In the 2nd stage, for each thickness of coating, the observed peak signal also occurs at lower time of flight as the process completes, however the rate of change is much less than during the first stage.

$$p_c = \sigma(\frac{1}{R_1} + \frac{1}{R_2}) \qquad \text{Equation 2}$$

Stage 3: During the stable 3rd stage, there are no further significant physical changes to the electrode layer with the density, porosity and thickness largely constant[36], and the peak signal ToF does not change with time.

These three stages can be identified by the change in the ultrasound peak ToF, and the distinct changes in the first two peak signals these can be monitored through ΔToF and Δ Intensity. In addition, the mass loss as the solvent is removed can be correlated to the ultrasound signal change. The following section elucidates these observations further.

As shown in Figure 4(a)] alongside the weight change of the anode coating during the DP which was recorded to monitor the solvent removal Figure 4 (b). The peak evolutions at each stage and the transition periods between 2nd and 3rd stage are shown plotted in Figure 4(c)-(f).

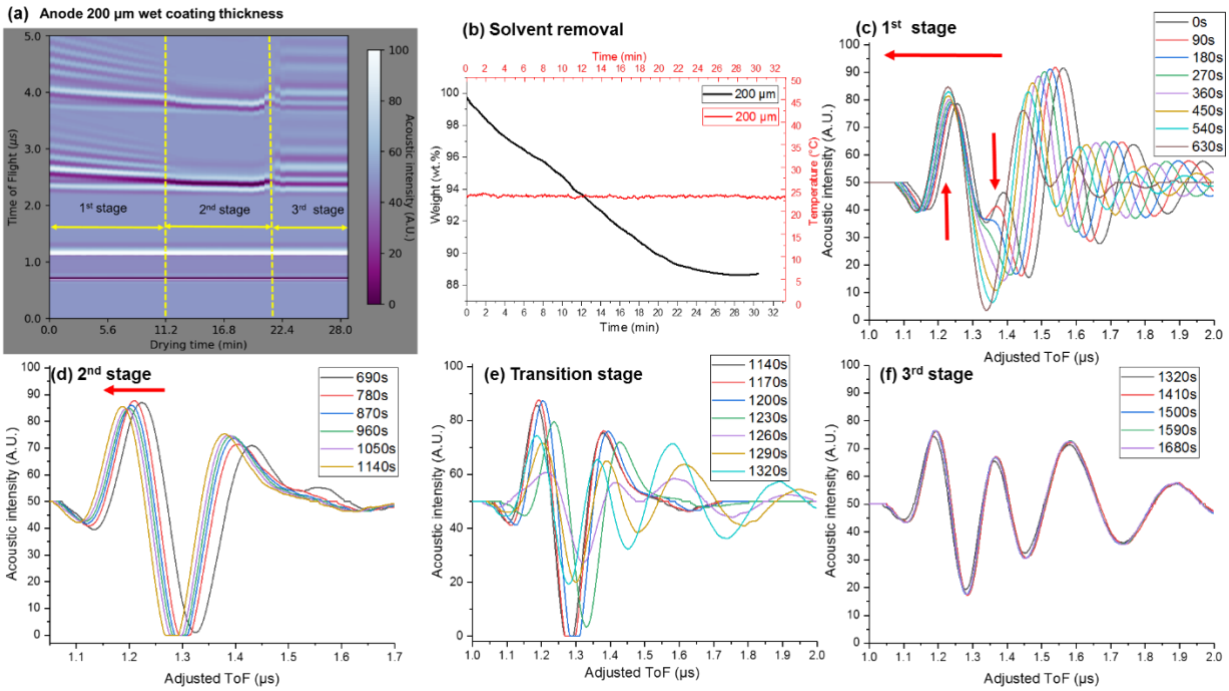

Figure 4 (a) Colour map of acoustic intensities and ToF during 200 µm anode coating layer drying at RT); (b) weight loss of solvent during anode slurry drying measured by digital balance; (c) acoustic ToF evolution during the 1st stage of drying; (d) acoustic ToF evolution during the 2nd stage of drying; (e) transition stage (acoustic ToF evolution between 2nd and 3rd stage of drying); (f) acoustic ToF evolution during the 3rd stage of drying.

Figure 4 (c) shows the acoustic ToF evolution in the 1st stage of drying corresponding to the colour map in Figure 4 (a) between 0-11 min. Here, the first two peaks shift to left which can be explained as the reflection of the ultrasonic wave at the interfaces in the different stages of drying and the thickness reduction of the coating. As the drying time increases, the electrode coating condenses until becoming a solid phase, that resulting in a faster response of the ultrasonic signal reflection due to higher material elastic moduli. This stage can correlate with the top-down film consolidation drying mechanism which was reported by Jaiser *et al.*[10]. The consolidation layer of the electrode is promptly formed at the surface of the coating, even at low elastic moduli of slurry with no sedimentation. As the drying continues more solvent is removed, this consolidation layer grows with expanding area until it approaches the substrate and spreads out the entre coating[36]. The similar results are observed for coating thicknesses at 250, 300 and 350 µm as shown in Figure 5(c), Figure 6(c), and Figure 7(c), respectively.

Figure 4(c) also shows that the intensity of first peak (ToF ~1.25 µs at 0s) increases and the second peak decreases (ToF ~1.4 µs at 0s) between 0-630s. These peak evolutions of

ultrasonic waves are resulted by the constant solvent evaporation, consequently result to film shrinkage and the coating layer become more condensed [13, 22]. The amplified intensity of the peak is due to the attenuation of the ultrasonic signal at the solid-liquid interface (occurring at the beginning of DP) which is much stronger than at the solid-solid interface (occurring at the later stage of DP). This is due to greater signal reflection and scattering at the solid-slurry interface compared to the solid-liquid interface[36].

Figure 4(d) shows the acoustic ToF evolution in the 2nd stage of drying for the anode coating thickness at 200 µm, which corresponding to the colour map in Figure 4 (a) between 11-20 min. The ultrasonic signal response has no significant change compared with the 1st stage in Figure 4(c) with slightly shift of ToF to the left. According to the gravimetric analysis in Figure 4(b), there is still weight loss between 11-20 min which correlates with the shift of ToF in the 2nd stage and is due to further solvent removal, During the 2nd stage, the pores between active material particles which were occupied by solvent are emptied. In this stage, the solvent evaporates at the internal gas-liquid interfaces and must then diffuse as vapour out of the film[7], that the density, elastic moduli of the anode coating film increases, therefore result in a faster response of the ultrasonic signal reflection[36]. The similar shifts of ultrasonic waves are also observed for drying the anode coating with thickness at 250 and 300 µm as shown in Figure 5 (d) and Figure 6 (d), respectively. Although there is a clear difference between stage 1 and 2 with the acoustic measurements, this is not seen in the gravimetric measurement which shows the advantage of using acoustic measurement over the standard gravimetric measurements.

In Figure 4 (e), the ultrasonic waves become fluctuating without any significant trends at drying time between 1140-1320s. The similar fluctuation happened for ~180s are observed for drying the electrode with thicker coating as shown in Figure 5 (e), Figure 6 (e), and Figure 7 (e). The fluctuation of the ultrasonic waves for all coating thickness is due to the significant physical change of the coatings that the interface between current collector and coating has completely become solid-solid interface. At the end of the transition/fluctuation stage, the 3rd stage of drying is very stable as shown in Figure 4 (f) which indicates the completion of the DP. For all coatings with different thicknesses, this transition phase happens at the same time that the gradient of the drying plot changes which is a good indication that the electrode is dried or entering the final stage of drying. The stable ultrasonic waves are also observed for other coating thickness as shown in Figure 5 (f), Figure 6 (f) and Figure 7 (f).

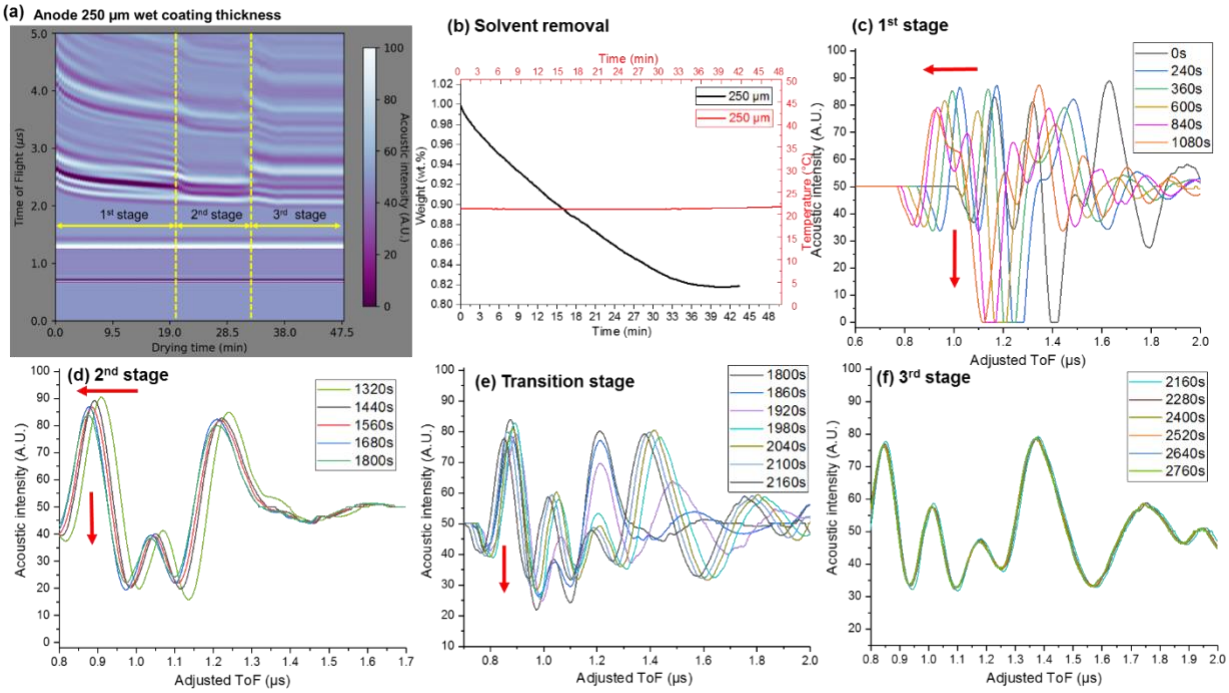

Figure 5 (a) Colour map of acoustic intensities and ToF during 250 µm anode coating layer drying at RT; (b) weight loss of solvent during anode slurry drying measured by digital balance; (c) acoustic ToF evolution during the 1st stage of drying; (d) acoustic ToF evolution during the 2nd stage of drying; (e) transition stage (acoustic ToF evolution between 2nd and 3rd stage of drying); (f) acoustic ToF evolution during the 3rd stage of drying.

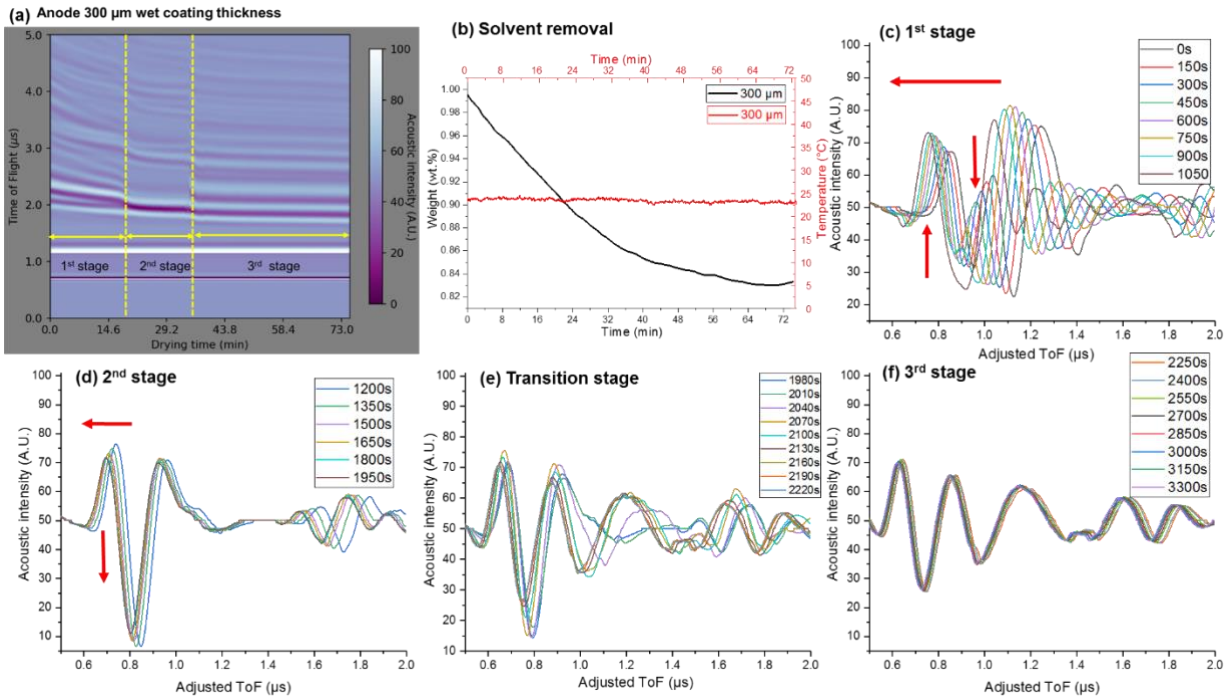

Figure 6 (a) Colour map of acoustic intensities and ToF during 300 µm anode coating layer drying at; (b) weight loss of solvent during anode slurry drying measured by digital balance; (c) acoustic ToF evolution during the 1st stage of drying; (d) acoustic ToF evolution during the 2nd stage of drying; (e) transition stage (acoustic ToF evolution between 2nd and 3rd stage of drying); (f) acoustic ToF evolution during the 3rd stage of drying.

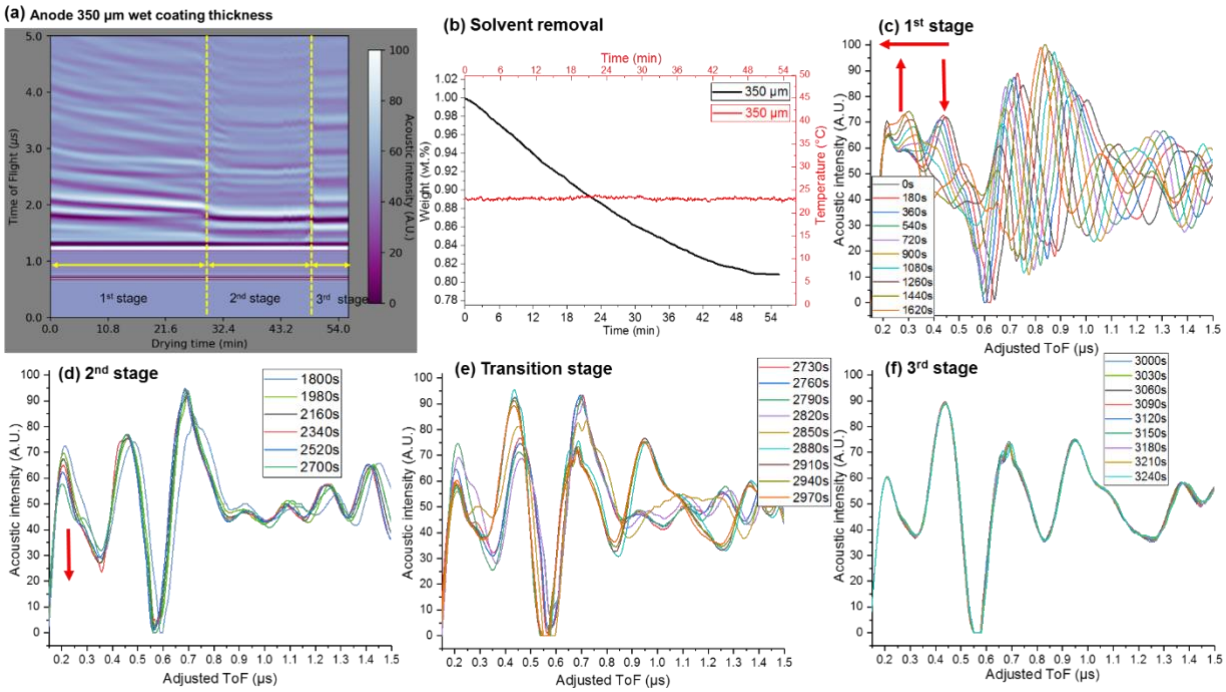

Figure 7 (a) Colour map of acoustic intensities and ToF during 350 µm anode coating layer drying at; (b) weight loss of solvent during anode slurry drying measured by digital balance; (c) acoustic ToF evolution colour map during the 1st stage of drying; (d) acoustic ToF evolution during the 2nd stage of drying; (e) transition stage (acoustic ToF evolution between 2nd and 3rd stage of drying); (f) acoustic ToF evolution during the 3rd stage of drying.

The completion of DP for anode with different coating thicknesses can also be supported by the gravimetric analysis, which the total drying time derived from ultrasound acoustic measurement that was calculated when there is no further change in the acoustic waveform as shown in Figure 8 (a) are consistent with the drying time derived from gravimetric analysis as shown in Figure 8 (b). In Figure 8(a), as the coating thickness increases from 200 to 350 µm, the total drying time increases from 1320 to 2640s. The total drying time derived from gravimetric analysis as shown in Figure 8(b) have the similar trend that the drying time increases from ~1400 to ~2700s. In addition to the total drying time, the ultrasound acoustic measurement can also provide more information for different stages of drying as shown in Figure 8 (a), where the drying time for 1st and 2nd stages are all increase with the increment of coating thickness. However, the 3rd stage transition [the fluctuation stage between 2nd and 3rd stage as shown in Figure 4 (e), Figure 5 (e), Figure 6 (e) and Figure 7 (e)] have no change at all coating thicknesses. The results prove the ultrasound acoustic measurement is an effective tool to not only monitor the entire drying time, but also provide the details of the physical evolution of the coating occurred during the DP by correlating the signal evolution with the current collector -coating interface changes.

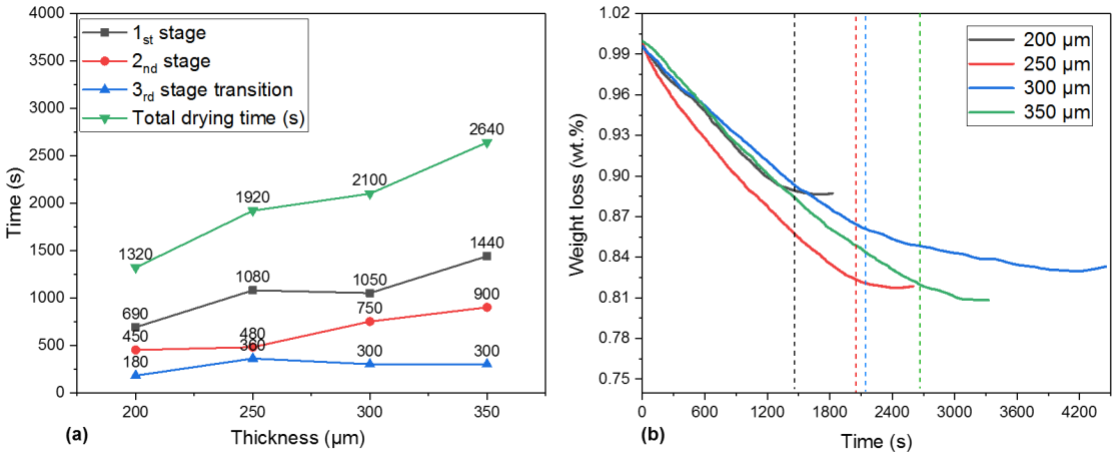

Figure 8 (a) Quantified time spent from acoustic measurement for each stage of drying at RT with anode coating layer at layer at 200, 250, 300 and 350 μm; (b) Thermo gravimetric analysis during anode slurry drying at RT with different coating thicknesses (the crossed points between the dotted lines and plots are indicate the total drying time).

To enhance the interpretation of ultrasonic signal evolution over the electrode DP, the discussions focus only on the first two reflective peaks which could indicate the interface revolution. For example, the current collector -solvent (solid-liquid) interface at the early stage of drying and current collector -solid particle (solid-solid) interface at the end of dying. In addition to the ToF shift and attenuation discussed early, more quantitative data are derived as shown in Figure 9 to guide the user to use ultrasound acoustic measurement to monitor the DP. The Δ ToF of the first two peaks for each stage of drying for all coating thicknesses are plotted in Figure 9 (a), (b) and (c), and the Δ Intensity are illustrated in Figure 9 (d), (e) and (f). In Figure 9 (a), the result showing the Δ ToF for different coating thickness for the first two peaks in 1st stage are in a similar trend. The similar results are also observed for 2nd stage and 3rd stage transition stage as shown in Figure 9 (b) and (c). Nevertheless, the Δ Intensity in Figure 9 (d), (e) and (f) are showing diverse trends which is due to the physical evolution of the electrode coating which make it difficult to identify the specific peaks. During the dynamic DP, the interfaces between current collector and electrode coating include the solid-liquid, solid-slurry and solid-solid interfaces[36], that will result to the disappearance of existing peaks and also appearance of new peaks. The finding still prove the feasibility of using ultrasound acoustic measurement to monitor the electrode DP, especially the ToF evolution is more indicative comparing with the evolution of intensity.

A possible application of using ultrasound acoustic measurement in the industrial electrode manufacturing process is to adjust the drying rate by reading the 2D colour map acquired during DP in a large scale of manufacturer. As there is no significant physical evolution happened in the 2nd and 3rd stages [as designated in Figure 4 (a), Figure 5 (a), Figure 6 (a)

and Figure 7 (a)] which will play less significant impact on the electrodes, therefore the drying rate could be increased at the beginning of 2nd stage to save the total drying time. The application of this technique would significantly save the time and cost for manufacturing LIB electrodes. The authors expect acoustic techniques will form a key part of the suite of diagnostic techniques routinely, which could be used to monitor electrochemical devices across various processes, including fabrication to aid the deployment of these devices in increasingly demanding applications.

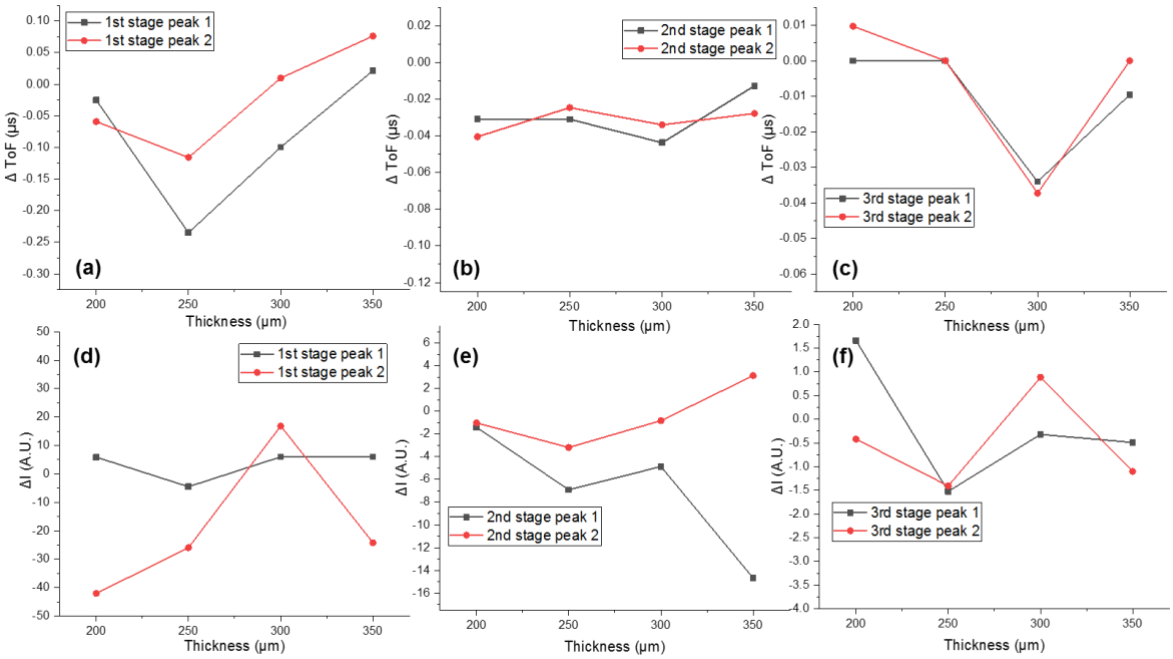

Figure 9 Acoustic ToF evolution during drying the anode with coating layer at 200, 250, 300 and 350 μm: (a)(b)(c) delta ToF; (d)(e)(f) delta intensity.

4 Conclusion

A developed ultrasound acoustic measurement has been applied in the LIB anode DP to monitor the physical evolution, especially the changes of current collector to coating interface. A series of different anode coating thickness (200, 250, 300 and 350 μm) have been studied with the same setup to investigate the correlation between acoustic signal attenuations (both vertical and horizontal shifts which represent the intensity and ToF evolutions) and coating thickness. The key findings are listed below:

- The results showing the similar ToF evolution during the DP regardless the coating thickness, that the 1st stage with the significant decrement of ToF, the ToF evolution in the 2nd stage is more mild compare with the 1st stage, and the 3rd stage is very stable. It is noticeable there is a transient period between 2nd and 3rd stages where the

observed signal response changes dramatically which last ~180s for all coating thicknesses.

- The completion of DP at the beginning of 3rd stage designated in colour maps for anode with different coating thicknesses has also been supported by the gravimetric analysis, which enable to validate the assumptions derived from ultrasonic signals.
- The further derived quantitative data (drying time and Δ ToF for each stage of drying) show the ultrasound acoustic measurement is an effective tool which is not only monitoring the total drying time, but also providing the drying time in each of drying stage. In the other word, the ultrasound acoustic measurement can provide the physical structure evolution of the coating during the DP by interpreting the signal evolution.
- A possible application of using ultrasound acoustic measurement in the industrial electrode manufacturing process is to increase drying rate at the beginning of 2nd stage to save drying time by reading the 2D colour map acquired during DP.

In conclusion, ultrasound acoustic measurement shows great potential to be implied in the electrode DP as an indicator to adjust faster drying to fabricate cost-effective LIB electrodes, and also provides the diagnostics of the electrode in the early stage of battery manufacturing chain.

Supporting Information. Supporting figure of overview of acoustic time of flight evolution during anode drying at room temperature with wet coating thickness

Acknowledgement

This work was supported by the Faraday Institution [EP/S003053/1 grant number FIRG015]. PRS would like to acknowledge the Royal Academy of Engineering (CiET1718\59) for financial support.

Author Contributions: Conceptualization, Y.S.Z. and D.J.L.B.; methodology, Y.S.Z.; software, A.N.P.R., R.E.O. and Y.S.Z.; validation, Y.S.Z. and J.B.R.; formal analysis, Y.S.Z.; investigation, Y.S.Z.; data curation, Y.S.Z.; writing-original draft preparation, Y.S.Z.; writing, R.E.O., J.L., J.O.M., and J.B.R.; visualization, Y.S.Z.; supervision, D.J.L.B, P.R.S. and E.K.; funding acquisition, D.J.L.B, P.R.S. and E.K.; All authors have read and agreed to the published version of the manuscript.

References:

(1) GVR, Lithium-ion Battery Market Size, Share & Trends Analysis Report By Product (LCO, LFP, NCA, LMO, LTO, Lithium Nickel Manganese Cobalt), *By Application, By Region, and Segment Forecasts, 2020 - 2027*; Grand View Research: 2020.
(2) Li, C.-C.; Wang, Y.-W. Binder Distributions in Water-Based and Organic-Based Licoo2 Electrode Sheets and Their Effects on Cell Performance. *Journal of the Electrochemical Society* **2011,** *158* (12), A1361-A1370.
(3) Lim, S.; Ahn, K. H.; Yamamura, M. Latex Migration in Battery Slurries During Drying. *Langmuir* **2013,** *29* (26), 8233-8244.
(4) Baunach, M.; Jaiser, S.; Schmelzle, S.; Nirschl, H.; Scharfer, P.; Schabel, W. Delamination Behavior of Lithium-ion Battery Anodes: Influence of Drying Temperature During Electrode Processing. *Drying Technology* **2016,** *34* (4), 462-473.
(5) Westphal, B.; Bockholt, H.; Günther, T.; Haselrieder, W.; Kwade, A. Influence of Convective Drying Parameters on Electrode Performance and Physical Electrode Properties. *ECS Transactions* **2015,** *64* (22), 57-68.
(6) Hagiwara, H.; Suszynski, W. J.; Francis, L. F. A Raman Spectroscopic Method to Find Binder Distribution in Electrodes During Drying. *Journal of Coatings Technology and Research* **2014,** *11* (1), 11-17.
(7) Jaiser, S.; Friske, A.; Baunach, M.; Scharfer, P.; Schabel, W. Development of A Three-Stage Drying Profile Based on Characteristic Drying Stages for Lithium-ion Battery Anodes. *Drying Technology* **2017,** *35* (10), 1266-1275.
(8) Jaiser, S.; Funk, L.; Baunach, M.; Scharfer, P.; Schabel, W. Experimental Investigation into Battery Electrode Surfaces: The Distribution of Liquid at The Surface and the Emptying of Pores During Drying. *Journal of Colloid and Interface Science* **2017,** *494*, 22-31.
(9) Jaiser, S.; Kumberg, J.; Klaver, J.; Urai, J. L.; Schabel, W.; Schmatz, J.; Scharfer, P. Microstructure Formation of Lithium-ion Battery Electrodes During Drying–an *Ex-Situ* Study Using Cryogenic Broad Ion Beam Slope-cutting and Scanning Electron Microscopy (Cryo-BIB-SEM). *Journal of Power Sources* **2017,** *345*, 97-107.
(10) Jaiser, S.; Müller, M.; Baunach, M.; Bauer, W.; Scharfer, P.; Schabel, W. Investigation of Film Solidification and Binder Migration During Drying of Li-ion Battery Anodes. *Journal of Power Sources* **2016,** *318*, 210-219.
(11) Müller, M.; Pfaffmann, L.; Jaiser, S.; Baunach, M.; Trouillet, V.; Scheiba, F.; Scharfer, P.; Schabel, W.; Bauer, W. Investigation of Binder Distribution in Graphite Anodes for Lithium-ion Batteries. *Journal of Power Sources* **2017,** *340*, 1-5.
(12) Pfaffmann, L.; Jaiser, S.; Müller, M.; Scharfer, P.; Schabel, W.; Bauer, W.; Scheiba, F.; Ehrenberg, H. New Method for Binder and Carbon Black Detection at Nanometer Scale in Carbon Electrodes for Lithium-ion Batteries. *Journal of Power Sources* **2017,** *363*, 460-469.
(13) Susarla, N.; Ahmed, S.; Dees, D. W. Modeling and Analysis of Solvent Removal During Li-ion Battery Electrode Drying. *Journal of Power Sources* **2018,** *378*, 660-670.
(14) Zhang, Y. S. A Review of Lithium-ion Battery Electrode Drying: Mechanisms and Metrology. *Advanced Energy Materials* **2021**.
(15) Kwade, A.; Haselrieder, W.; Leithoff, R.; Modlinger, A.; Dietrich, F.; Droeder, K. Current Status and Challenges for Automotive Battery Production Technologies. *Nature Energy* **2018,** *3* (4), 290-300.
(16) Kaiser, J.; Wenzel, V.; Nirschl, H.; Bitsch, B.; Willenbacher, N.; Baunach, M.; Schmitt, M.; Jaiser, S.; Scharfer, P.; Schabel, W. Process and Product Development of Electrodes for Lithium-ion Cells. *Chemie Ingenieur Technik* **2014,** *86* (5), 695-706.
(17) Günther, T.; Billot, N.; Schuster, J.; Schnell, J.; Spingler, F. B.; Gasteiger, H. A. In the Manufacturing of Electrodes: Key process for the future success of lithium-ion batteries, *Advanced Materials Research*, Trans Tech Publ: 2016; pp 304-311.
(18) Zheng, H.; Tan, L.; Liu, G.; Song, X.; Battaglia, V. S. Calendering Effects on the Physical and Electrochemical Properties of Li [Ni1/3Mn1/3Co1/3] O_2 Cathode. *Journal of Power Sources* **2012,** *208*, 52-57.

(19) Garsany, Y.; Singer, I. L.; Swider-Lyons, K. E. Impact of Film Drying Procedures on RDE Characterization of Pt/VC Electrocatalysts. *Journal of Electroanalytical Chemistry* **2011,** *662* (2), 396-406.
(20) Hwang, S.-W.; Hyun, S.-H. Synthesis and Characterization of Tin Oxide/Carbon Aerogel Composite Electrodes for Electrochemical Supercapacitors. *Journal of Power Sources* **2007,** *172* (1), 451-459.
(21) Liu, W.-w.; Yan, X.-b.; Lang, J.-w.; Peng, C.; Xue, Q.-j. Flexible and Conductive Nanocomposite Electrode Based on Graphene Sheets and Cotton Cloth for Supercapacitor. *Journal of Materials Chemistry* **2012,** *22* (33), 17245-17253.
(22) Stein, M.; Mistry, A.; Mukherjee, P. P. Mechanistic Understanding of the Role of Evaporation in Electrode Processing. *Journal of The Electrochemical Society* **2017,** *164* (7), A1616-A1627.
(23) Luo, H.; Cardinal, C. M.; Scriven, L. E.; Francis, L. F. Ceramic Nanoparticle/Monodisperse Latex Coatings. *Langmuir* **2008,** *24* (10), 5552-5561, DOI: 10.1021/la800050u.
(24) Ma, Y.; Davis, H. T.; Scriven, L. E. Microstructure Development in Drying Latex Coatings. *Progress in Organic Coatings.* **2005,** *52* (1), 46-62.
(25) Buss, F.; Roberts, C. C.; Crawford, K. S.; Peters, K.; Francis, L. F. Effect of Soluble Polymer Binder on Particle Distribution in A Drying Particulate Coating. *Journal of Colloid and Interface Science* **2011,** *359* (1), 112-120,.
(26) Hawley, W. B.; Li, J. Electrode Manufacturing for Lithium-ion Batteries: Analysis of Current and Next Generation Processing. *Journal of Energy Storage* **2019,** *25*, 100862.
(27) Kusano, T.; Hiroi, T.; Amemiya, K.; Ando, M.; Takahashi, T.; Shibayama, M. Structural Evolution of A Catalyst Ink for Fuel Cells During the Drying Process Investigated by CV-SANS. *Polymer Journal* **2015,** *47* (8), 546-555.
(28) Krebs, F. C. Polymer Solar Cell Modules Prepared Using Roll-to-roll Methods: Knife-over-edge Coating, Slot-die Coating and Screen Printing. *Solar Energy Materials and Solar Cells* **2009,** *93* (4), 465-475.
(29) Lim, S.; Kim, S.; Ahn, K. H.; Lee, S. J. Stress Development of Li-ion Battery Anode Slurries During the Drying Process. *Industrial & Engineering Chemistry Research* **2015,** *54* (23), 6146-6155.
(30) Higa, K.; Zhao, H.; Parkinson, D. Y.; Barnard, H.; Ling, M.; Liu, G.; Srinivasan, V. Electrode Slurry Particle Density Mapping Using X-ray Radiography. *Journal of The Electrochemical Society* **2017,** *164* (2), A380-A388.
(31) Majasan, J.; Robinson, J.; Owen, R.; Maier, M.; Radhakrishnan, A. N. P.; Pham, M.; Tranter, T. G.; Zhang, Y.; Shearing, P.; Brett, D. Recent Advances in Acoustic Diagnostics for Electrochemical Power Systems. *Journal of Physics: Energy* **2021**.
(32) Hsieh, A.; Bhadra, S.; Hertzberg, B.; Gjeltema, P.; Goy, A.; Fleischer, J. W.; Steingart, D. A. Electrochemical-acoustic Time of Flight: In *Operando* Correlation of Physical Dynamics with Battery Charge and Health. *Energy & Environmental Science* **2015,** *8* (5), 1569-1577.
(33) Davies, G.; Knehr, K. W.; Van Tassell, B.; Hodson, T.; Biswas, S.; Hsieh, A. G.; Steingart, D. A. State of Charge and State of Health Estimation Using Electrochemical Acoustic Time of Flight Analysis. *Journal of The Electrochemical Society* **2017,** *164* (12), A2746-A2755.
(34) Robinson, J. B.; Maier, M.; Alster, G.; Compton, T.; Brett, D. J.; Shearing, P. R. Spatially Resolved Ultrasound Diagnostics of Li-ion Battery Electrodes. *Physical Chemistry Chemical Physics* **2019,** *21* (12), 6354-6361.
(35) Deng, Z.; Huang, Z.; Shen, Y.; Huang, Y.; Ding, H.; Luscombe, A.; Johnson, M.; Harlow, J. E.; Gauthier, R.; Dahn, J. R. Ultrasonic Scanning to Observe Wetting and “Unwetting” in Li-ion Pouch Cells. *Joule* **2020,** *4* (9), 2017-2029.
(36) Zhang, Y. S. *In-Situ* Ultrasound Acoustic Measurement of The Lithium-ion Battery Electrode Drying Process. *ACS Applied Materials & Interfaces* **2021,** *13* (30), 36605–36620.
(37) Kendrick, E. Advancements in Manufacturing. In *Future Lithium-ion Batteries*; 2019; pp 262-289.
(38) Wood, D. L.; Quass, J. D.; Li, J.; Ahmed, S.; Ventola, D.; Daniel, C. Technical and Economic Analysis of Solvent-based Lithium-ion Electrode Drying with Water and NMP. *Drying Technology* **2018,** *36* (2), 234-244.

(39) Li, J.; Du, Z.; Ruther, R. E.; An, S. J.; David, L. A.; Hays, K.; Wood, M.; Phillip, N. D.; Sheng, Y.; Mao, C. Toward Low-cost, High-energy Density, and High-power Density Lithium-ion Batteries. *Jom* **2017,** *69* (9), 1484-1496.
(40) Tsotsas, E.; Mujumdar, A. S. *Modern Drying Technology*, Wiley Online Library: 2007.
(41) Whitaker, S. Flow in Porous Media I: A Theoretical Derivation of Darcy's Law. *Transport in porous media* **1986,** *1* (1), 3-25.
(42) Hubbert, M. K. Darcy's Law and the Field Equations of the Flow of Underground Fluids. *Hydrological Sciences Journal* **1957,** *2* (1), 23-59.
(43) Siqveland, L. M.; Skjæveland, S. M. Derivations of the Young-Laplace Equation. **2021**.